ACS APPLIED MATERIALS & INTERFACES

Research Article

www.acsami.org

Electric Papers of Graphene-Coated Co_3O_4 Fibers for High-Performance Lithium-Ion Batteries

Xiaoling Yang,[†,*] Kaicai Fan,[†] Yihua Zhu,[†,*] Jianhua Shen,[†] Xin Jiang,[†] Peng Zhao,[†] Shaorong Luan,[§] and Chunzhong Li[†]

[†]Key Laboratory for Ultrafine Materials of Ministry of Education, School of Materials Science and Engineering, and [§]Research Center of Analysis and Test, School of Chemistry and Molecular Engineering, East China University of Science and Technology, 130 Meilong Road, Shanghai 200237, China

Supporting Information

ABSTRACT: A facile strategy to synthesize the novel composite paper of graphene nanosheets (GNS) coated Co_3O_4 fibers is reported as an advanced anode material for high-performance lithium-ion batteries (LIBs). The GNS were able to deposit onto Co_3O_4 fibers and form the coating via electrostatic interactions. The unique hybrid paper is evaluated as an anode electrode for LIBs, and it exhibits a very large reversible capacity (~840 mA h g^{-1} after 40 cycles), excellent cyclic stability and good rate capacity. The substantially excellent electrochemical performance of the graphene/Co_3O_4 composite paper is the result from its unique features. Notably, the flexible structure of graphenic scaffold and the strong interaction between graphene and Co_3O_4 fibers are beneficial for providing excellent electronic conductivity, short transportation length for lithium ions, and elastomeric space to accommodate volume varies upon Li^+ insertion/extraction.

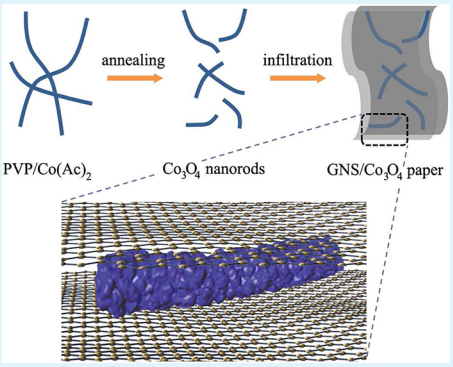

KEYWORDS: *graphene paper, Co_3O_4 fiber, anode, lithium-ion batteries*

1. INTRODUCTION

Rechargeable lithium ion batteries (LIBs) have attracted a tremendous amount of attention in the scientific and industrial fields because they are currently the dominant power source for popular consumer electronics and the most promising candidate to power the upcoming electric vehicles.[1−3] So far, various electrode materials with a high charge/discharge rate and a high reversible capacity have been extensively investigated.[4,5] Transition metal oxides such as Fe_3O_4,[6] MoO_2,[7] CuO,[8] and Co_3O_4[9] exploited as the anode materials for LIBs have attracted extensive interest due to their higher theoretical specific capacity (ca. 700−1000 mA h g^{-1}) than the commercial graphite (372 mA h g^{-1}).[10,11] In contrast to the intercalation mechanism,[12] the transition metal oxides operate based on the conversion reaction from metal oxides to small metal clusters with the oxygen reacting with Li^+ to form Li_2O.[13] Hence, upon lithiation/delithiation during cycling, the oxides suffer large volume expansion/contraction and severe particle aggregation, leading to a large irreversible capacity loss and poor cycling stability.[14,15] Therefore, it still remains a challenge to develop simple and effective synthetic strategies to fabricate high-performance metal oxides electrodes with high reversible capacity and long cycle life.

To overcome these disadvantages, various porous structures such as nanospheres,[16] porous nanotubes,[17] or bundle-like nanostructure[18] have been synthesized. The assembled porous architectures can provide an elastic buffer space to accommodate the volume expansion/contraction of active materials during Li insertion/extraction process, thus maintaining large capacity, good cycling stability and high rate capability.[19] Moreover, carbon coating has been widely used to prevent the exfoliation of the active materials and facilitate the electron transportation in the electrodes, thus reduce the reversible capacity loses during Li^+ insertion/extraction.[20,21] Graphene, which is a new two-dimensional carbon material, is becoming one of the most appealing matrices to integrate with other nanoparticles for LIBs due to its superior electrical conductivity, large surface area (2630 m^2 g^{-1}), excellent structural flexibility and high thermal and chemical stability.[22] Importantly, the graphene nanosheets (GNS) not only can preserve the high electric conductivity of the overall electrode but also can effectively prevent the volume expansion/extraction and the aggregation of metals or metal oxides during charge/discharge processes.[23] Electrode construction consisting of graphene paper-like structure could facilitate faster Li ion and electron transfer and significantly reduces polarization, thereby resulting in enhanced electrochemical performance.[24] In particular, graphene/metal or graphene/metal oxides composites paper have been produced by integrating 3D graphenic scaffold with guest nanoparticles and assembly.[25] However, these flexible graphene sheets could not ensure effect electrical contact between the active materials and interconnected graphene,

Received: November 13, 2012
Accepted: January 15, 2013
Published: January 15, 2013

which causes inferior Li ion accessibility and thus modest improvement in the cell performance. Kang et al[26] have demonstrated the efficient fabrication of composite papers of GNS coated cellulose fibers, in which GNS coating forms a continuous network through a bridge of cellulose fibers, providing a high electric conductivity. Therefore, the self-assembly of 2D graphene into 3D heterogeneous structures is particularly promising for establishing improved electrode.

Herein, we developed a facile strategy to fabricate 3D hierarchical structures of GNS/Co_3O_4 fibers composite papers by dispersing Co_3O_4 fibers in GNS solution and followed by infiltration (Figure. 1). The electrospun Co_3O_4 fibers are coated

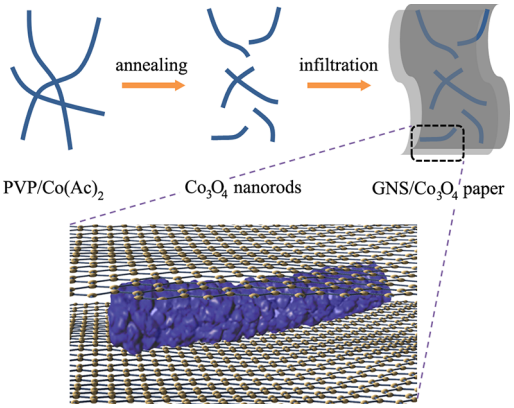

Figure 1. Fabrication of GNS/Co_3O_4 fiber composite paper.

by the graphene sheets and embedded in 3-D graphenic scaffold, forming paper-like structure. The composite paper not only ensure solid contact between the Co_3O_4 fibers and the GNS, but also facilitate electron transport, and renders the elastomeric space needed to accommodate the volume variation of Co_3O_4 upon Li^+ insertion/extraction. In addition, the assembled porous fiber architecture can relieve the volume variations during the Li^+ insertion/extraction process, which contributes to the excellent electrochemical performance. Thus, when used in LIBs, this GNS/Co_3O_4 fibers composite paper exhibits a very large capacity, high rate capability, and excellent cycling stability.

2. EXPERIMENTAL SECTION

2.1. Reagents and Materials. All the chemicals were of analytical grade and used without any further purification. Polyvinylpyrrolidone (PVP; MW = 1 300 000) was purchased from Sigma-Aldrich Chemicals Co. 3-Aminopropyltrimethoxysilane (APS) was purchased from J&K Chemical Ltd. And all other chemicals were purchased from Shanghai Chemical Reagent Co. Ultrapure water (18 MΩ cm) was used for all experiments.

2.2. Instruments. Scanning electron microscope (SEM) images were taken by using a JEOL JSM-6360LV microscopy. Transmission electron microscope (TEM) images were taken on a JEOL JEM 2011 microscope (JEOL, Japan) at an acceleration voltage of 200 kV. The crystalline structure was investigated by X-ray power diffraction (RIGAK, D/MAX 2550 VB/PC, Japan). Raman spectra were recorded on an inVia Raman microprobe (Renishaw Instruments, England) with 785 nm laser excitation.

2.3. Synthesis and Preparation. Co_3O_4 fibers were initially prepared by electrospinning technique.[27] In a typical procedure, 1 g of polyvinylpyrrolidone (PVP) polymer was added to 9 mL of ethanol, and stirred at room temperature for few hours to form homogeneous solution. Then, 0.8 g of Cobalt(II) acetate tetra hydrate ($Co(Ac)_2$) were added to the above solution with stirring for 3 h. Subsequently, using a voltage of 10 kV applied between the electrospinning jet and the collector, with a distance of 10 cm and at a flow rate of 2 mL/h, the as-prepared solution was electrospun into nanofibers. To remove the solvent residuals, the as-prepared PVP/$Co(Ac)_2$ composite fibers were dried in an oven at 60 °C for several hours. Then, the Co_3O_4 fibers were obtained after annealing at 450 °C for 5 h in an atmospheric environment.

Graphene oxides were prepared by the modified Hummers method.[28,29] To integrate graphene sheets and Co_3O_4 fibers into an assembly, the Co_3O_4 fibers were first modified by APS. The prepared GO suspensions were dispersed in water (4 mg mL^{-1}) by a sonication process. pH control is very critical for fabricating the final continuous GNS/Co_3O_4 composite paper. Both the GO solution and the modified Co_3O_4 fibers (25:75 in weight ratio) were first mixed at pH 8. The GNS/Co_3O_4 composite papers were fabricated by filtering the above mixed solution through membrane filters (0.22 um) by vacuum suction. During the filtration, the pH value of the solution was adjusted to 4 to make both components oppositely charged, and thus triggered by the electrostatic interactions between both components,[30] the assembled GNS/Co_3O_4 composite paper was left in the filtration apparatus and immediately carried through hydrazine reduction. For comparison, the pure graphene paper was prepared in a similar process without Co_3O_4 fibers.

2.4. Electrochemical Measurements. For the testing of GNS/Co_3O_4 composite paper and graphene paper, the working electrode was prepared by directly pressing a piece of sample paper onto the Cu current collector. For comparison, the traditional working electrodes were prepared by a slurry coating procedure. The slurry was obtained by mixing the active materials (Co_3O_4), acetylene black, and polyvinylidene fluoride (PVDF) at a weight ratio of 80:10:10 in N-methylpyrrolidinone. This slurry was uniformly pasted onto Cu foils and dried at 80 °C for 12 h in vacuum to remove the remove the solvent. Electrochemical measurements were performed using Swagelok-type cells with Lithium foil as the counter/reference electrode, Celgard 2400 membrane as the separator. The electrolyte was a 1 M $LiPF_6$ solution in a 50: 50 (w: w) mixture of ethylene carbonate (EC) and diethyl carbonate (DMC). The cells were assembled in argon-filled glovebox. Cyclic voltammetry was performed on a CHI660D electrochemical workstation over the potential range of 0.01−3.00 V vs Li^+/Li at a scan rate of 0.1 mV s^{-1}. Galvanostatic cycling test were performed in a LAND-CT2001A test system at a voltage window of 0.01−3.00 V at current density of 100 mA g^{-1}. To test rate performance, the electrodes were first cycled at current density of 100 mA g^{-1} for 5 cycles, and the current was increased in stages to 200, 300, 500, and 1000 mA g^{-1}. Here the total weight of the GNS/Co_3O_4 composite paper was used to calculate the capacity values.

3. RESULTS AND DISCUSSION

3.1. Characterization of GNS/Co_3O_4 Composite Paper. Figure 2a shows the typical X-ray diffraction (XRD) profile of the bare Co_3O_4 fibers and the GNS/Co_3O_4 composite paper. Compared to that of bare Co_3O_4 fibers, an additional broad and small diffraction peak appears at around 23° for GNS/Co_3O_4 composite paper, which can be indexed into the disorderedly staked GNS.[31] The interlayer distance between sheets calculated according to Bragg's equation is close to but lager than the d_{002}-spacing of graphite (3.35 Å). The increased d-spacing for GNS/Co_3O_4 composite paper can be ascribed to the presence of a small amount of oxygen-containing functional groups and the existence of Co_3O_4 fibers.[32] All the other peaks are also observed in the Co_3O_4 fibers and assigned to the well-crystallized Co_3O_4 with a face-centered cubic (fcc, $Fd3m$ (227), a = 0.808 nm) structure (JCPDS no.42−1467). In the Raman spectra of GNS/Co_3O_4 composite paper (Figure 2b), the characteristic D band at ∼1345 cm^{-1} and the G band at ∼1596 cm^{-1} are observed for the GNS/Co_3O_4 composite paper. In

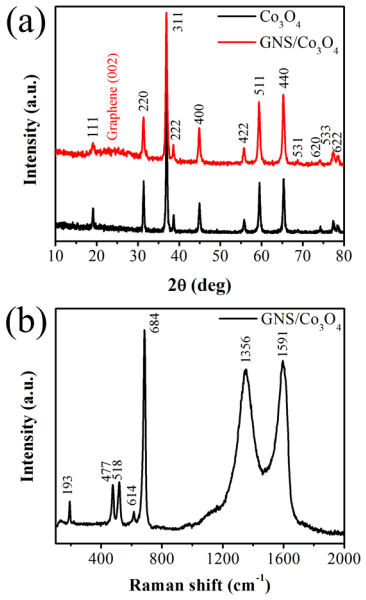

Figure 2. (a) Wide-angle XRD patterns of Co_3O_4 fibers and GNS/Co_3O_4 composite paper. (b) Raman spectra of GNS/Co_3O_4 composite paper.

addition, the peaks of Raman shift at 191, 486, 525, 603, and 686 cm^{-1} correspond to the E_g, $F^{12}{}_m$, $F^{22}{}_g$ and A_{1g} vibration modes of Co_3O_4. These results demonstrate the existence of both graphene and well-crystallized Co_3O_4. For quantifying the amount of Co_3O_4 in the GNS/Co_3O_4 composite paper, thermogravimetric analysis (TGA) was carried out in air (see Figure S2 in the Supporting Information). Clearly, the weight of graphene is almost lost before 700 °C. The result reveals that the Co_3O_4 content in the GNS/Co_3O_4 composite paper is estimated to be 78.3%.

Figure. 3a shows the scanning electron microscopy (SEM) of the electrospun $Co(Ac)_2$/PVP fibers. As observed, the composite fibers exhibit ultrafine fiber morphology and smooth surface. The average diameter of fibers can range from 700 to 800 nm. After annealing at 450 °C, Co_3O_4 fiber are formed due to the oxidative decomposition of $Co(Ac)_2$ and removal of

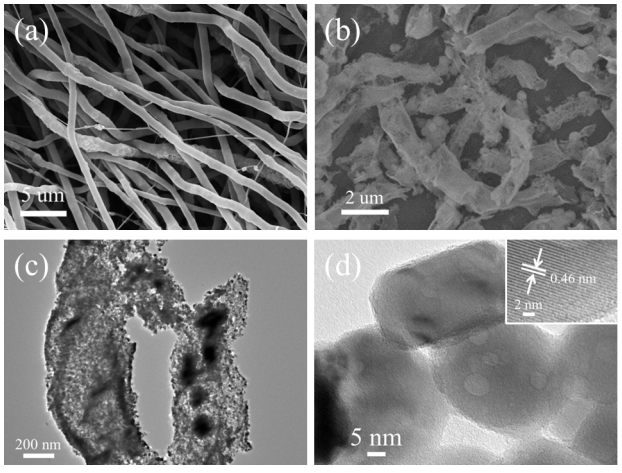

Figure 3. (a) SEM image of electrospun $Co(AC)_2$/PVP fibers. (b) SEM image of Co_3O_4 fibers after annealed at 450 °C. (c) TEM image of Co_3O_4 fibers after annealed at 450 °C. (d) HRTEM image showing the lattice fringe of Co_3O_4.

PVP. The average diameter of the resultant Co_3O_4 fibers decreases to about 600 nm (Figure 3b). The TEM image (Figure 3c) demonstrates that the fibers consist of numerous interconnected Co_3O_4 nanocrystals forming the mesoporous structure. The periodic fringe spacing of 0.46 nm is shown in Figure 3d, which agrees with the (111) lattice of cubic Co_3O_4, and it further confirms the high crystallinity of the Co_3O_4 fibers.

The structure of GNS/Co_3O_4 composite paper was characterized by SEM to provide the micrographs in Figure 4. As shown in Figure 4a, the cross-section of GNS/Co_3O_4

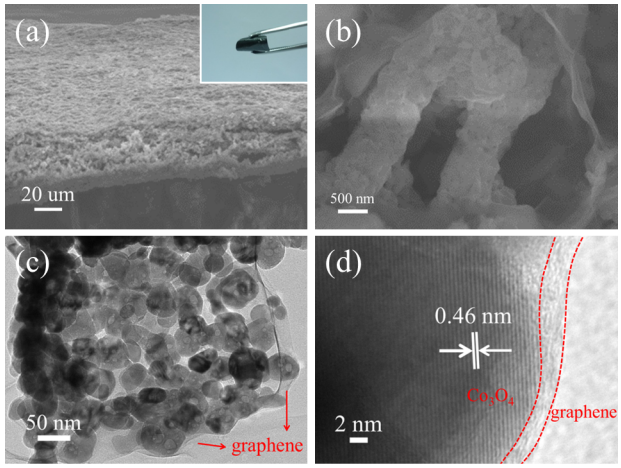

Figure 4. (a) SEM image of the cross-section of a GNS/Co_3O_4 composite paper; inset shows the digital image of a GNS/Co_3O_4 composite paper. (b) Enlarged cross-sectional view of the paper. (c) TEM image of GNS/Co_3O_4 composite paper. (d) HRTEM image of GNS/Co_3O_4 composite paper.

composite paper revealed uniform thickness (~20 μm). And because of the existence of Co_3O_4 fibers, the sheets appeared more crumpled, and pocketed the void space. The porosity promotes the diffusion of Li ions in the electrode and enables the achievement of high-rate capability. A higher magnification SEM image revealed the core–shell structure and graphene sheets are indeed tightly attached onto the Co_3O_4 fibers (Figure 4b). Besides, some free graphene sheets reconstitute graphite to serve as the highly conductive channels between Co_3O_4, which decreases the inner resistance of electrodes and is favorable for stabilizing the electronic conductivity. The SEM images of top surfaces sections revealed homogeneously dispersed Co_3O_4 fibers coated by reassembled graphene sheets (see Figure S1 in the Supporting Information). Overall, the graphene coated Co_3O_4 core–shell fibers are embedded in a 3D graphenic scaffold. The N_2 adsorption/desorption isotherms of the final products is shown in Figure S3. The BET specific surface area of the final products was 43.2 m^2 g^{-1}. The high specific surface area could be attributed to the formation of secondary pores between Co_3O_4 fibers and graphene sheets, and is believed to be beneficial to the enhancement of its electrochemical performance.

To provide further insights into the morphology and structure on the resulting GNS/Co_3O_4 composite paper, TEM investigations were carried out. The TEM images confirmed the Co_3O_4 fibers were well-coated by the extremely thin and flexible GNS via electrostatic interactions (Figure 4c). Figure 4d shows the HRTEM image taken from the edge of graphene-coated Co_3O_4 fibers. The well-resolved lattice fringes are clearly observed along the (111) zone axis of Co_3O_4. The

dx.doi.org/10.1021/am302685t | ACS Appl. Mater. Interfaces 2013, 5, 997–1002

interplanar spacing of ~0.37 nm corresponds to the separation between (002) lattice planes of graphite. This further confirmed that the Co_3O_4 fibers are well coated by few layer GNS.[33] However, it is unlikely that the graphene forms continuous layers on the surface of the particle. Lithium ions can still easily penetrate the few-layer structure and react with Co_3O_4 particles for electrochemical reaction to take place. In this unique structure, a portion of the graphene sheets reconstitute graphite to form a continuous, highly conducting 3D network, and the presence of the graphene stacks on the surface of the particle most likely provides good conductivity and also prevents the agglomeration of the individual Co_3O_4 fibers.[34]

3.2. Electrochemical Properties of GNS/Co_3O_4 Composite Paper. The unique structure endows the GNS/Co_3O_4 composite paper electrodes with excellent lithium story capacity, which was evaluated using various electrochemical tests. Cyclic voltammetry (CV) experiments were fist conducted to investigate the electrochemical performance at a scanning rate of 0.1 mV s^{-1} over the voltage range 0.01−3.00 V (Figure. 5). In the first cycle, the main cathodic peak was observed at around 0.50 V, which can arise from the electrochemical reduction (lithiation) reaction of Co_3O_4 with Li^+ and the formation of solid electrolyte interphase (SEI) films. The observed dominant anodic peak at 2.24 V was ascribed to the oxidation (delithiation) reaction of Co_3O_4.[35] Because of the hysteresis in the CV technique, the cathodic peak negatively shifted, and the anodic peak positively shifted compared to the discharge/charge voltage plateaus (Figure 6a).[36] The lithium storage mechanism of Co_3O_4 can be described by the electrochemical conversion reaction: $Co_3O_4 + 8Li \rightarrow 4Li_2O + 3Co$.[37] During the subsequent cycles, the main reduction peak is shifted to 0.86 V, peak intensity drops significantly in the second cycle, indicating the occurrence of some irreversible processes in the electrode material in the first cycle. On the other hand, the oxidation peak at ~2.2 V in the anodic sweep exhibits little change in the first three cycles, indicating a good reversibility of the electrochemical reaction.[38] The CV behavior confirms the overall capacity of GNS/Co_3O_4 composite paper arises mainly from the properties of the metal oxide, and further indicates that the electrochemical reversibility is gradually built after the initial cycle.

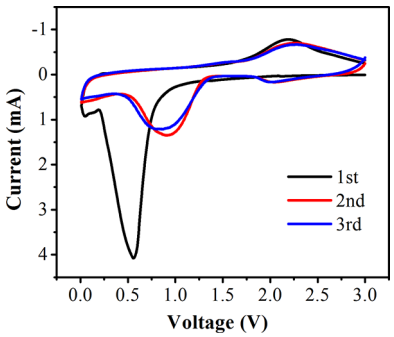

Figure 5. Cyclic voltammograms of the GNS/Co_3O_4 composite paper electrode at a scan rate of 0.1 mV s^{-1} for three cycles.

To highlight the superiority of the unique GNS/Co_3O_4 composite paper for anode materials of LIBs, we evaluated the electrochemical performance of the free-standing GNS/Co_3O_4 composite paper, G paper, and traditional Co_3O_4 electrode for Li insertion/extraction using galvanostatic cycling in a Swagelok-type cell with Li metal as the counter electrode. The cell was charge/discharge at a current density of 100 mA g^{-1} over the range of 0.01 and 3.00 V vs Li^+/Li. Figure 6 shown the charge/discharge profiles of the conventional Co_3O_4 electrode, G paper and GNS/Co_3O_4 composite paper in the first and second cycles. In the first discharge step, no voltage plateau was observed for graphene, and the voltage profiles were similar for both the Co_3O_4 fibers and GNS/Co_3O_4 composite paper. The two similar voltage curves in the first cycle presented a well-defined long voltage plateau at ca.0.9−

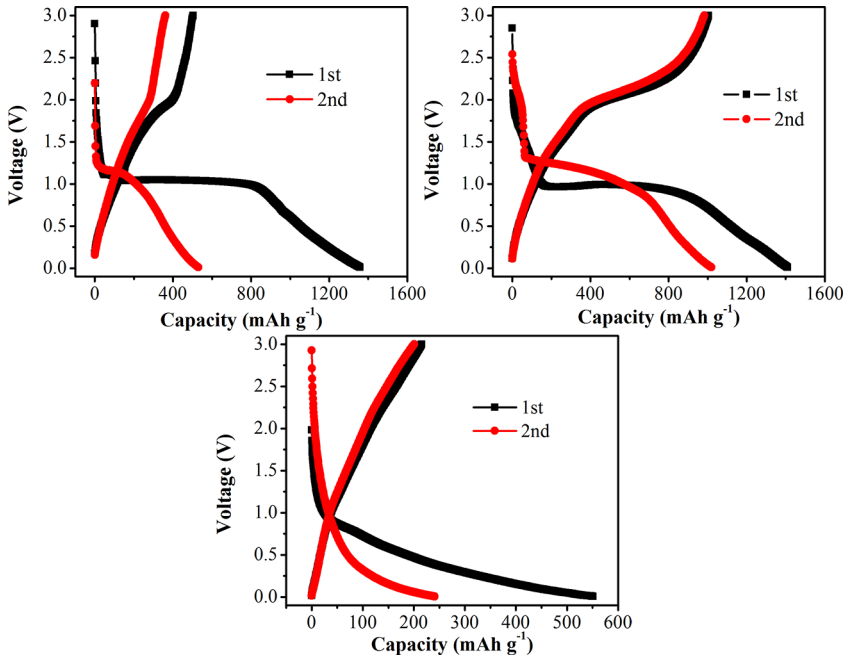

Figure 6. Frst and second cycle of discharge/charge profiles for different samples: (a) traditional Co_3O_4 electrode, (b) G paper, (c) GNS/Co_3O_4 composite paper. The current density is 100 mA g^{-1}.

dx.doi.org/10.1021/am302685t | ACS Appl. Mater. Interfaces 2013, 5, 997−1002

1.0 V associated with the conversion from Co_3O_4 to an intermediate-phase CoO (or $Li_xCo_3O_4$) and then to metallic Co, followed by a sloping curve down to the voltage of 0.01 V, indicative of typical characteristics of voltage trends for the Co_3O_4 electrode.[39] It is observed that the initial discharge and charge capacities are 1356.3 and 500 mA h g^{-1} for the conventional Co_3O_4 electrode, 550.2 and 216.1 mA h g^{-1} for the graphene paper electrode, and 1404.8 and 1005.7 mA h g^{-1} for GNS/Co_3O_4 composite paper. The initial capacity loss may result from the incomplete conversion reaction and irreversible lithium loss due to the formation of solid electrolyte interphase layer.[35] Compared to the theoretical capacity of bulk Co_3O_4 (890 mA h g^{-1}), the extra capacity in initial cycles probably contributed to the larger electrochemical active surface area of graphene and grain boundary area of the Co_3O_4 fibers.[40]

Figure 7a shows the cyclic performances of conventional Co_3O_4 electrode, G papers, and GNS/Co_3O_4 composite paper,

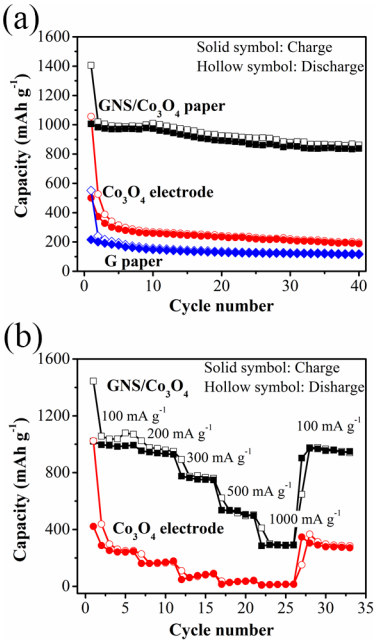

Figure 7. (a) Cyclic performances of electrodes fabricated by traditional Co_3O_4 electrode, G paper, GNS/Co_3O_4 composite paper at current rate of 100 mA g^{-1}. (b) Charge−discharge performances of Co_3O_4 electrode, GNS/Co_3O_4 composite paper at various current rates.

respectively. Since the second cycle, the GNS/Co_3O_4 composite paper exhibits much better electrochemical lithium storage performance than graphene paper and Co_3O_4 electrode. After the first cycle, GNS/Co_3O_4 composite paper maintains the reversible capacity well and exhibits a high reversible capacity of 840 mA h g^{-1} after 40 cycles, whereas it can be seen that the reversible capacity of graphene paper and Co_3O_4 decreases from 525 to only 194 mA h g^{-1} and from 218 to 110 mA h g^{-1}, respectively, up to 40 cycles. In addition, the Coulombic efficiency of GNS/Co_3O_4 composite paper rapidly rises from 71.6% in the first cycles to 96.4% in the second one and then remains above 95% in the following cycles, indicating very good reversibility (see Figure S4 in the Supporting Information). From Figures 6 and 7a, it is important to note that the enhanced cycling stability of the paper can be ascribed to the flexible GNS/Co_3O_4 composite paperlike structure that favors fast electron and ion transport, providing an elastic buffer space to accommodate the volume change and preventing the aggregation of the nanoparticles and the cracking or crumbling of the electrode material upon lithium-ion insertion/extraction.[41] In addition to the high reversible capacity, the GNS/Co_3O_4 composite paper exhibited a much better rate capacity compared to the traditional Co_3O_4 electrode cycled at various rates between 100 and 1000 mA g^{-1} (Figure 7b). For example, the specific capacity of GNS/Co_3O_4 composite paper at a current density of 300 mA g^{-1} is as high as 754 mA h g^{-1}, whereas the reversible capacity of traditional Co_3O_4 electrode rapidly drops 76 mA h g^{-1}. Moreover, the GNS/Co_3O_4 composite paper electrode can still deliver a high capacity of 295 mA h g^{-1} at a rate of 1000 mA g^{-1}, whereas the Co_3O_4 cannot store charges any more. Importantly, after the high-rate measurements, the specific capacities of the GNS/Co_3O_4 composite paper electrode cycled at 100 mA g^{-1} were able to recover to the initial reversible values, implying their good reversibility.

The highly reversible capacity, good cyclic performance, and enhanced rate capacity, may be attributed to the unique hierarchical of the GNS/Co_3O_4 composite paperlike structure. First, the graphene sheets in the composite papers have an enhanced conductivity compared to the custom Co_3O_4 electrode.[42] Moreover, the graphene sheets can serve as the continuous conductive channels between Co_3O_4 fibers, which decrease the inner resistance of LIBs and are favorable for stabilizing the electronic conductivity. Second, the loose stacking of the graphene sheets induced by the presence of Co_3O_4 fibers enables good electrolyte penetration. This is beneficial to give rise to a large contact area between the active material and the electrolyte, and thus provides fast transport pathways and large accessible sites on the surface of active materials for electrolyte ions.[43] Third, the flexible two-dimensional graphene sheets encapsulated Co_3O_4 fibers architecture not only can accommodate the volume change and suppress the aggregation of Co_3O_4 upon Li^+ insertion/extraction, but also can efficiently prevents the cracking or crumbling of the electrode materials. Therefore, an excellent cyclic performance can be expected. Moreover, the unique porous rod-like architecture made of interconnected Co_3O_4 nanocrystals is beneficial to buffer the strain from the volume change during the charge/discharge processes, thus leading to the enhanced cylability.[44] The above synergetic effects arising from conducting graphene sheets, Co_3O_4 fibers and the unique 3D paperlike structure is responsible for the excellent electrochemical performance of the overall electrode through the maximum utilization of the electrochemically active materials.

4. CONCLUSION

In conclusion, we have demonstrated a facile strategy to synthesize the novel GNS/Co_3O_4 composite paper. The GNS was deposited onto the Co_3O_4 fibers and forms a coating under controlled infiltration. Therefore, the flexible structure of graphenic scaffold and the strong interaction between graphene and Co_3O_4 fibers are beneficial for efficiently preventing volume expansion/contraction and aggregation of Co_3O_4 during the Li charge/discharge process. Therefore, such a composite paper is capable of effectively utilizing the good conductivity, mechanical flexibility, and good electrochemical performance of graphene as well as the large electrode/electrolyte contact area, and short path length for Li transport. When used as an anode material LIBs, this material exhibits a

dx.doi.org/10.1021/am302685t | ACS Appl. Mater. Interfaces 2013, 5, 997−1002

very large reversible capacity, excellent cyclic stability, and good rate capacity. Finally, we believe this binder free 3D hierarchical GNS/metal oxides composites paper exhibits a high electrochemical activity as an electrode in supercapacitor or lithium ion batteries with a promising electrochemical performance.

■ ASSOCIATED CONTENT

Supporting Information

Figures S1−S4. This material is available free of charge via the Internet at http://pubs.acs.org.

■ AUTHOR INFORMATION

Corresponding Author

*Tel.: +86-21-64252022. Fax: +86-21-64250624. E-mail: xlyang@ecust.edu.cn (X.Y.) yhzhu@ecust.edu.cn (Y.Z.).

Notes

The authors declare no competing financial interest.

■ ACKNOWLEDGMENTS

We thank the National Natural Science Foundation of China (21236003, 21206042, 20925621, 20976054, and 21176083), the Fundamental Research Funds for the Central Universities, and the Program for Changjiang Scholars and Innovative Research Team in University (IRT0825), and the Shanghai Leading Academic Discipline Project (project number: B502) for financial supports.

■ REFERENCES

(1) Kang, K.; Meng, Y. S.; Breger, J.; Grey, C. P.; Ceder, G. *Science* **2006**, *311*, 977−979.
(2) Arico, A. S.; Bruce, P.; Scrosati, B.; Tarascon, J.; Schalkwijk, W. V. *Nat. Mater.* **2005**, *4*, 366−377.
(3) Ji, L.; Lin, Z.; Alcoutlabi, M.; Zhang, X. *Energy Environ. Sci.* **2011**, *4*, 2682−2699.
(4) Wang, H.; Yang, Y.; Liang, Y.; Robinson, T.; Li, Y.; Robinson, J. T.; Li, Y.; Jackson, A.; Cui, Y.; Dai, H. *Nano Lett.* **2011**, *11*, 2644−2647.
(5) Chen, D.; Mei, X.; Lu, M.; Xie, J.; Lu, J.; Lee, J. M. *Angew. Chem., Int. Ed.* **2012**, *51*, 2409−2414.
(6) Zhou, G.; Wang, D. W.; Li, F.; Zhang, L.; Li, N.; Wu, Z. S.; Wen, L.; Lu, G. Q.; Cheng, H. Q. *Chem. Mater.* **2010**, *22*, 5306−5313.
(7) Sun, Y.; Hu, X.; Luo, W.; Huang, Y. *ACS Nano* **2011**, *5*, 7100−7107.
(8) Ko, S.; Lee, J.; Yang, H. S.; Park, S.; Jeong, U. *Adv. Mater.* **2012**, *24*, 4451−4456.
(9) Zhu, J.; Sharma, Y. K.; Zeng, Z.; Zhang, X.; Srinivasan, M.; Mhaisalkar, S.; Zhang, H.; Hng, H. H.; Yan, Q. *J. Phys. Chem. C* **2011**, *115*, 8400−8406.
(10) Cabana, J.; Monconduit, L.; Larcher, D.; Palacín, M. R. *Adv. Mater.* **2010**, *22*, E170−E192.
(11) Liang, J.; Wei, W.; Zhong, D.; Yang, Q.; Li, L.; Guo, L. *ACS Appl. Mater. Interfaces* **2012**, *4*, 454−459.
(12) Maloney, R. P.; Kim, H. J.; Sakamoto, J. S. *ACS Appl. Mater. Interfaces* **2012**, *4*, 2318−2321.
(13) Kang, E.; Jung, Y. S.; Cavanagh, A. S.; Kim, G.; George, S. M.; Dillon, A. C.; Kim, J. M.; Lee, J. *Adv. Funct. Mater.* **2011**, *21*, 2430−2438.
(14) Yuan, S. M.; Li, J. X.; Yang, L. T.; Su, L. W.; Liu, L.; Zhou, Z. *ACS Appl. Mater. Interfaces* **2011**, *3*, 705−709.
(15) Yan, N.; Hu, Y.; Li, Y.; Wang, Y.; Zhong, H.; Hu, X.; Kong, X.; Chen, Q. *J. Phys. Chem. C* **2012**, *116*, 7227−7235.
(16) Li, C. C.; Yin, X. M.; Li, Q. H.; Chen, L. B.; Wang, T. H. *Chem.—Eur. J.* **2011**, *17*, 1596−1604.
(17) Luo, W.; Hu, X.; Sun, Y.; Huang, Y. *J. Mater. Chem.* **2012**, *22*, 8916−8921.
(18) Wang, L.; Cheng, W.; Gong, H.; Wang, C.; Wang, D.; Tang, K.; Qian, Y. *J. Mater. Chem.* **2012**, *22*, 11297−11302.
(19) Wang, X.; Tian, W.; Zhai, T.; Zhi, C.; Bando, Y.; Golberg, D. J. *Mater. Chem.* **2012**, *22*, 23310−23326.
(20) Xiong, S.; Chen, J. S.; Lou, X. W.; Zeng, H. C. *Adv. Funct. Mater.* **2012**, *22*, 861−871.
(21) Wang, X.; Guan, H.; Chen, S.; Li, H.; Zhai, T.; Tang, D.; Bando, Y.; Golberg, D. *Chem. Commun.* **2011**, *47*, 12280−12282.
(22) Yin, S.; Zhang, Y.; Kong, J.; Zou, C.; Li, C. M.; Lu, X.; Ma, J.; Boey, F. Y. C.; Chen, X. *Acs Nano* **2011**, *5*, 3831−3838.
(23) Wang, C.; Du, G.; Stahl, K.; Huang, H.; Zhong, Y.; Jiang, J. Z. *J. Phys. Chem. C* **2012**, *116*, 4000−4011.
(24) Li, B.; Cao, H.; Shao, J.; Li, G.; Qu, M.; Yin, G. *Inorg. Chem.* **2011**, *50*, 1628−1632.
(25) Lee, J. K.; Smith, K. B.; Hayner, C. M.; Kung, H. H. *Chem. Commun.* **2010**, *46*, 2025−2027.
(26) Kang, Y. R.; Li, Y. L.; Hou, F.; Wen, Y. Y.; Su, D. *Nanoscale* **2012**, *4*, 3248−3253.
(27) Cherian, C. T.; Sundaramurthy, J.; Kalaivani, M.; Ragupathy, P.; Kumar, P. S.; Thavasi, V.; Reddy, M. V.; Sow, C. H.; Mhaisalkar, S. G.; Ramakrishna, S.; Chowdari, B. V. R. *J. Mater. Chem.* **2012**, *22*, 12198−12924.
(28) Zhao, J.; Pei, S.; Ren, W.; Gao, L.; Cheng, H. *ACS Nano.* **2010**, *4*, 5245−5252.
(29) Shen, J. H.; Zhu, Y. H.; Zhou, K. F.; Yang, X. L.; Li, C. Z. *J. Mater. Chem.* **2012**, *22*, 545−550.
(30) Choi, B. G.; Yang, M.; Hong, W. H.; Choi, J. W.; Huh, Y. S. *ACS Nano* **2012**, *6*, 4020−4028.
(31) Qiu, J.; Zhang, P.; Ling, M.; Li, S.; Liu, P.; Zhao, H.; Zhang, S. *ACS Appl. Mater. Interfaces* **2012**, *4*, 3636−3642.
(32) Kim, H.; Seo, D. H.; Kim, S. W.; Kim, J.; Kang, K. *Carbon* **2011**, *49*, 326−332.
(33) Lee, J. S.; You, K. H.; Park, C. B. *Adv. Mater.* **2012**, *24*, 1084−1088.
(34) Chen, D.; Ji, G.; Ma, Y.; Lee, J. Y.; Lu, J. *ACS Appl. Mater. Interfaces* **2011**, *3*, 3078−3083.
(35) Wang, X.; Wu, X. L.; Guo, Y. G.; Zhong, Y.; Cao, X.; Ma, Y.; Yao, J. *Adv. Funct. Mater.* **2010**, *20*, 1680−1686.
(36) Lian, P.; Zhu, X.; Xiang, H.; Li, Z.; Yang, W.; Wang, H. *Electrochim. Acta* **2010**, *56*, 834−840.
(37) Xiong, S.; Chen, J. S.; Lou, X. W.; Zeng, H. C. *Adv. Funct. Mater.* **2012**, *22*, 861−871.
(38) Mei, W.; Huang, J.; Zhu, L.; Ye, Z.; Mai, Y.; Tu, J. *J. Mater. Chem.* **2012**, *22*, 9315−9321.
(39) Wu, Z. S.; Ren, W.; Wen, L.; Gao, L.; Zhao, J.; Chen, Z.; Zhou, G.; Li, F.; Cheng, H. M. *ACS Nano* **2010**, *4*, 3187−3194.
(40) Yang, X.; Fan, K.; Zhu, Y.; Shen, J.; Jiang, X.; Zhao, P.; Li, C. *J. Mater. Chem.* **2012**, *22*, 17278−17283.
(41) Wang, X.; Cao, X.; Bourgeois, L.; Guan, H.; Chen, S.; Zhong, Y.; Tang, D. M.; Li, H.; Zhai, T.; Li, L.; Bando, Y.; Golberg, D. *Adv. Funct. Mater.* **2012**, *22*, 2682−2690.
(42) Choi, B.; Chang, S.; Lee, Y.; Bae, J.; Kim, H.; Huh, Y. *Nanoscale* **2012**, *4*, 5924−5930.
(43) Luo, S.; Wang, K.; Wang, J.; Jiang, K.; Li, Q.; Fan, S. *Adv. Mater.* **2012**, *24*, 2294−2298.
(44) Wang, Y.; Xia, H.; Lu, L.; Lin, J. *ACS Nano* **2010**, *4*, 1425−1432.